

3D Imaging of Gap Plasmons in Vertically Coupled Nanoparticles by EELS Tomography

Georg Haberfehlner,^{*,†,‡,§} Franz-Philipp Schmidt,^{‡,§} Gernot Schaffernak,[§] Anton Hörl,[§] Andreas Trügler,[§] Andreas Hohenau,[§] Ferdinand Hofer,^{†,‡} Joachim R. Krenn,[§] Ulrich Hohenester,[§] and Gerald Kothleitner^{†,‡}

[†]Graz Centre for Electron Microscopy, Steyrergasse 17, 8010 Graz, Austria

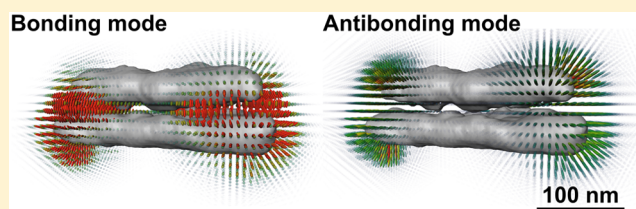
[‡]Institute of Electron Microscopy and Nanoanalysis, Graz University of Technology, Steyrergasse 17, 8010 Graz, Austria

[§]Institute of Physics, University of Graz, Universitätsplatz 5, 8010 Graz, Austria

Supporting Information

ABSTRACT: Plasmonic gap modes provide the ultimate confinement of optical fields. Demanding high spatial resolution, the direct imaging of these modes was only recently achieved by electron energy loss spectroscopy (EELS) in a scanning transmission electron microscope (STEM). However, conventional 2D STEM-EELS is only sensitive to components of the photonic local density of states (LDOS) parallel to the electron trajectory. It is thus insensitive to specific gap modes, a restriction that was lifted with the introduction of tomographic 3D EELS imaging. Here, we show that by 3D EELS tomography the gap mode LDOS of a vertically stacked nanotriangle dimer can be fully imaged. Besides probing the complete mode spectrum, we demonstrate that the tomographic approach allows disentangling the signal contributions from the two nanotriangles that superimpose in a single measurement with a fixed electron trajectory. Generally, vertically coupled nanoparticles enable the tailoring of 3D plasmonic fields, and their full characterization will thus aid the development of complex nanophotonic devices.

KEYWORDS: Plasmonics, nanoparticles, electron tomography, electron energy loss spectroscopy, photonic LDOS



Gap plasmonics deals with extreme light concentration in narrow gap regions of coupled metallic nanoparticles.¹ The fields in the gap region become strongly enhanced by coupled plasmon modes, giving rise to a myriad of novel effects, such as single-molecule strong coupling² and surface-enhanced Raman scattering,³ nonlinear optics,⁴ nanolasing,⁵ or plasmon-induced tunneling.^{6,7} Unfortunately, the diffraction limit of light forbids the direct optical observation of fields confined to nanometer dimensions, so that indirect measurements of the modification of the properties of quantum emitters placed in the gap region^{2,3} or of the plasmonic spectra⁸ have to be applied.

In recent years, electron energy loss spectroscopy (EELS) in a scanning transmission electron microscope (STEM) has been established as an ideal tool for direct observation of plasmonic fields at the nanoscale.⁹ In EELS, a swift electron interacts with plasmonic fields, losing a tiny fraction of its kinetic energy. By raster scanning the electron beam over a nanoparticle, one obtains a map of the photonic local density of states (LDOS)¹⁰ with subnanometer spatial resolution. However, in these maps the fields are integrated along the electron propagation direction, masking specific LDOS components, and in many cases EELS can be even blind to strong fields in the gap region.¹¹ Plasmon tomography can overcome this issue and retrieve the full 3D photonic LDOS distributions from a tilt

series of EELS maps. Earlier work demonstrated the proof of principle,^{12,13} but the approach was bound to the quasistatic approximation and other simplifications. In more recent work, we have extended the scheme such that it can be applied to nanoparticles of arbitrary size¹⁴ and have demonstrated its capability of mapping the full three-dimensional photonic LDOS of single and laterally coupled plasmonic modes through the solution of an inverse problem.¹⁵

In this Letter, we go one step further and apply our tomography scheme to 3D gap plasmonics, imaging the gap modes of vertically coupled nanoparticles and comparing the EELS results to optical extinction spectra. The interpretation of conventional 2D EELS data from such stacked geometries is hindered by the integral effect of the beam along its trajectory, when passing through or near the different layers and therefore requires a tomographic approach. From an application point of view, going from 2D to 3D structures by vertically stacking nanoparticles opens a wealth of new opportunities.^{16–18} First, coupling between two particles is no more limited to be mediated by single corners or edges but can extend over the whole structure. Second, very small gaps between two separate

Received: July 13, 2017

Revised: October 3, 2017

Published: October 5, 2017

particles are possible in a vertical arrangement, as thin film deposition can be readily controlled with subnanometer accuracy. Finally, the combination of lateral and vertical arrangements of nanoparticles opens further venues for the tailoring of 3D plasmonic fields.

We fabricated triangular silver/silicon dioxide/silver dimers (heights 20 nm/10 nm/20 nm) of different lateral sizes using electron beam lithography and vacuum evaporation on 5 nm thick silicon nitride substrates. The particle side lengths range from 140 to 340 nm. We use a single lithographically structured polymer mask for all three deposition steps which ensures the alignment of the different layers on top of each other. Triangles were chosen as their dipolar modes can be quite easily distinguished from higher order modes based on 2D EELS maps, but similar results are expected for other geometries, such as disks or squares. High-angle annular dark-field (HAADF) STEM images of four dimers of different size (labeled T1 through T4 with increasing sizes of 140, 190, 240, and 340 nm) and the 3D morphologies of the two smallest dimers (T1 and T2) as reconstructed from HAADF STEM tomography are shown in Figure 1. For this tomography

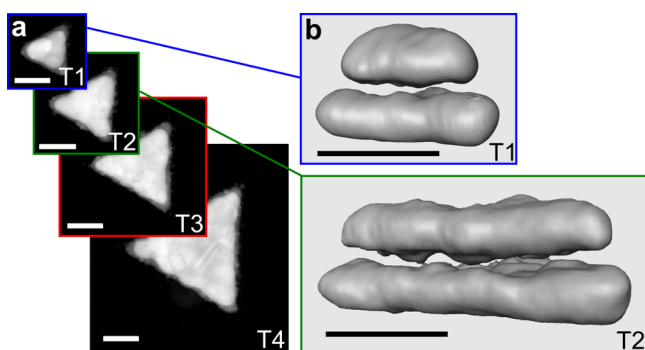


Figure 1. Morphology of 3D dimers: (a) HAADF STEM images of four silver 3D dimers of different sizes, labeled T1 to T4 with increasing size. (b) 3D reconstructions of the two smallest dimers T1 and T2. Scale bars are 100 nm.

reconstruction a 3D total-variation minimization algorithm was employed, which allows accurate reconstruction of the particles morphology even for a limited tilt range.^{19,20} In the 3D reconstruction, it can be seen that the two silver triangles are well separated by the insulating layer. The upper triangle is slightly smaller than the lower one due to material deposition on the edges of the mask opening, which reduces its size during the deposition process.

We recorded optical extinction spectra and EELS spectrum images of 3D dimers of different sizes to reveal the plasmon resonances of the structures. Figure 2a shows extinction spectra of arrays of four 3D dimers, with the sizes of the larger three dimers matching those of T1–T3 to within ± 20 nm. Figure 2b shows deconvolved EELS spectra summed over the full spectrum image for the T1–T4 samples and Figure 2c depicts the corresponding EELS maps extracted at the resonance energies. In the extinction spectra, a distinct strong peak shifts to lower energies with an increasing triangle size. A weaker peak is observed at lower energies for the two smallest dimers. For the two larger dimers this peak is red-shifted to energies out of the range of the optical spectrometer. In the EELS measurements, two resonance peaks are observed for all four 3D dimers due to the higher spectral measurement range. The two peaks are separated by 0.5–0.7 eV, depending on particle size, and

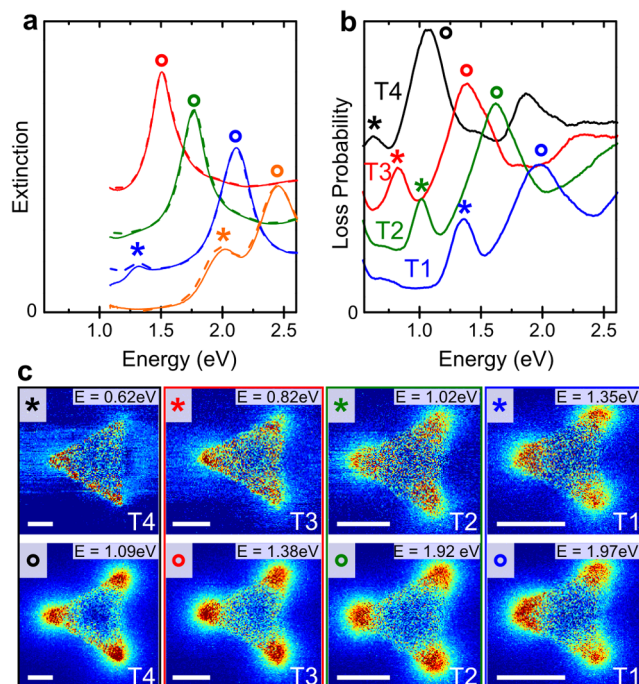


Figure 2. Dipole resonances on 3D dimers: (a) Optical extinction spectra of four 3D dimers. The two orthogonal polarizations (horizontal and vertical with respect to the triangle orientation in c) are shown by the solid and dashed (mostly overlapping) lines. For the two smaller 3D dimers (blue and orange lines) two resonance peaks are visible (labeled * and O); for the larger 3D dimers (green and red lines) the low energy peak (*) shifts out of the range of the spectrometer. (b) EELS spectra summed over the full spectrum images taken from T1 to T4 showing two resonance peaks (* and O) for all dimers, colors indicate particles of approximately same size. (c) 2D EELS maps extracted from the peak positions indicated in panel b. Curves in a and b are bare shifted by a constant offset relative to orange and blue curves, respectively. Scale bars are 100 nm.

shift to lower energies with increasing particle size. The peak positions match well in the optical and EELS measurements, small differences in peak position being most likely due to size differences, chemical and structural changes in the silver between deposition and measurement.²⁰

The EELS maps extracted at the peak energies in Figure 2b can be attributed to dipolar excitations.^{21,22} In Figure S1 we compare this data to EELS maps from a single triangle, which shows only a single dipole resonance.²³ Simulations of optical and electron beam excitations using the boundary element method (MNPBEM toolbox)^{24,25} on single nanoparticles and dimers also confirm the splitting of the dipolar mode (Figures S2 and S3). This splitting can be attributed to the coupling of the dipole modes on the lower and upper triangles and their hybridization into a bonding and an antibonding configuration.¹⁷ It is important to note that from the 2D EELS maps of the dipolar modes in Figure 2c it is impossible to determine the plasmon field profile, that is, the respective locations of LDOS features on the individual stacked triangles. In particular, there is no possibility for determining the magnitude of the gap modes. To clearly image the two observed dipolar modes a tomographic approach is mandatory.

For this purpose, we acquire a tilt series of EELS spectrum images from the two smallest 3D dimers (T1 and T2) over a range of about $\pm 75^\circ$. From the measured spectrum images in Figure 3, it becomes apparent that also from individual tilted

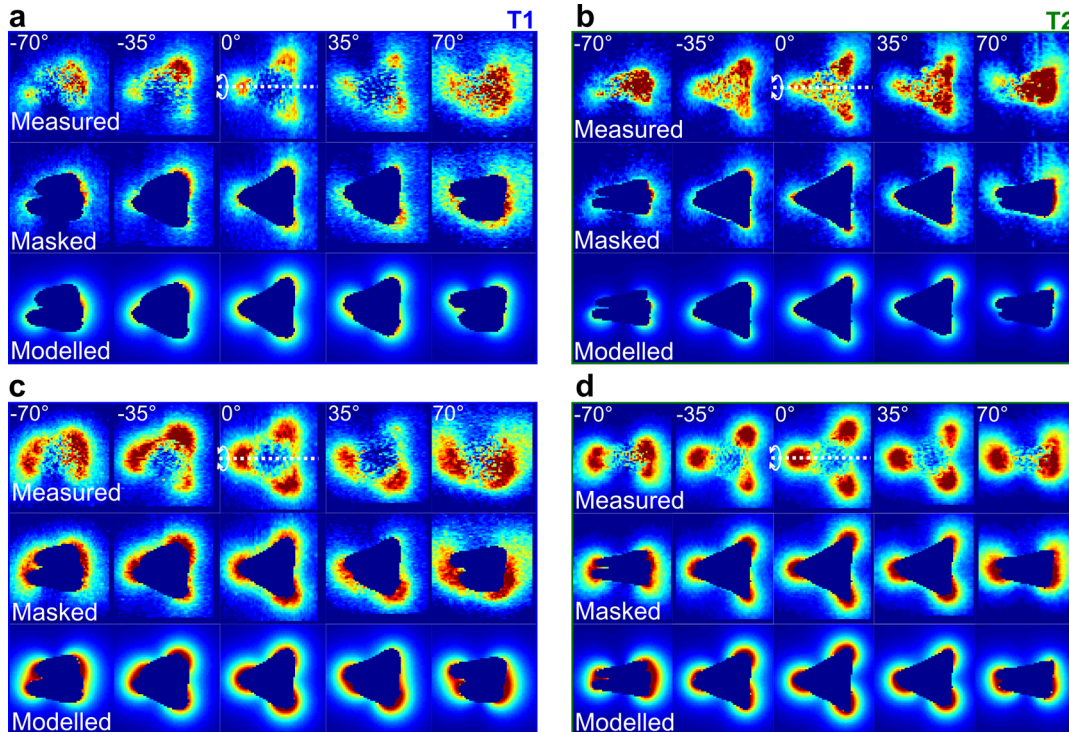


Figure 3. Comparison of measured and reprojected (modeled) EELS maps for five tilt angles as indicated, for the low-energy dipole mode (bonding) on (a) the dimer T1 and (b) the dimer T2 and for the high energy dipole mode (antibonding) on (c) T1 and (d) T2. For each mode the top row shows the measured (zero-loss normalized and deconvolved) data. The second row shows only data points at least 5 nm away from the particle, which are taken into account for the reconstruction. The lowest row shows the modeled (reprojected) maps, which result from the reconstruction. In the 0° projections the tilt axis is indicated.

EELS maps the plasmon modes cannot be clearly derived. Using the approach presented in ref 15, we reconstruct the dyadic Green tensor for both dipole modes on both dimers. As input for the reconstruction we use the experimental EELS maps and an eigenmode decomposition, which is based on the reconstructed 3D morphology of the nanoparticles.²⁶ For the reconstruction only the measured EELS data for beam trajectories outside of the particle are taken into account (Figure 3, masked data). We use a compressed sensing algorithm, which at the same time minimizes the difference between reprojected maps (Figure 3, modeled data) and experimental EELS maps and provides a basis with a minimal number of eigenmodes. After minimization, the dyadic Green tensor \mathbf{G} and, in turn, the photonic LDOS for the resonant modes at any position \mathbf{r} around the dimers are computed through

$$\rho_{\mathbf{n}}(\mathbf{r}) = \frac{6\omega}{\pi c^2} \text{Im}\{\mathbf{n} \cdot \mathbf{G}(\mathbf{r}, \mathbf{r}) \cdot \mathbf{n}\} \quad (1)$$

The photonic LDOS describes the coupling between a quantum emitter (e.g., fluorescent molecule or quantum dot) with dipole moment \mathbf{d} oriented along direction \mathbf{n} and the photonic environment.²⁷ Its definition is based on the relation between the electric field at a position \mathbf{r}' and the dipole source via the dyadic Green tensor

$$\mathbf{E}(\mathbf{r}') = \omega^2 \mu_0 \mathbf{G}(\mathbf{r}', \mathbf{r}) \cdot \mathbf{d} \quad (2)$$

Figure 4 and Movie S1 show the reconstructed photonic LDOS for both modes and for the two 3D dimers T1 and T2. The reconstructed LDOS around the dimers is displayed by pencils, where color and length represent the magnitude, and

the orientation indicates the direction along which the LDOS is maximal. For both modes and both dimers we observe that the photonic LDOS is highest around the corners of the triangles, as expected for dipolar excitations. For the lower energy modes (Figure 4a,b) we find that the LDOS in the gap region between the triangles is oriented in the vertical direction, so the corresponding electric field lines point from one triangle to the other one. This shows that this mode corresponds to a bonding configuration (with respect to the charge distribution). For the higher energy mode (Figure 4c,d) the LDOS in the gap is oriented in the horizontal direction, proving the antibonding configuration with equal repulsing charges on the two triangles.

Interestingly, the highest fields are present inside the gap for the bonding mode. This may appear slightly surprising, as the bonding mode is less pronounced in the 2D maps, as compared to the antibonding mode (Figure 2). However, the complex interplay between the local fields and the measured EELS maps, which cannot be interpreted as simple projections, has to be taken into account. Even though there is a large component of the LDOS along the beam direction locally inside the gap for the bonding mode at 0° tilt, the integral effect of interactions along the beam trajectory still leads to lower values of the EELS maps for the bonding mode as compared to the antibonding mode. Only through the full 3D reconstruction of the photonic LDOS, a quantitative comparison of the LDOS of the different modes becomes possible.

Especially for the smaller dimer, it can be observed that the asymmetry of the structure influences the spatial distribution of the LDOS. With the lower triangle being larger, the LDOS of the bonding mode is higher around the lower triangle as the resonance energy of the bonding mode is closer to the

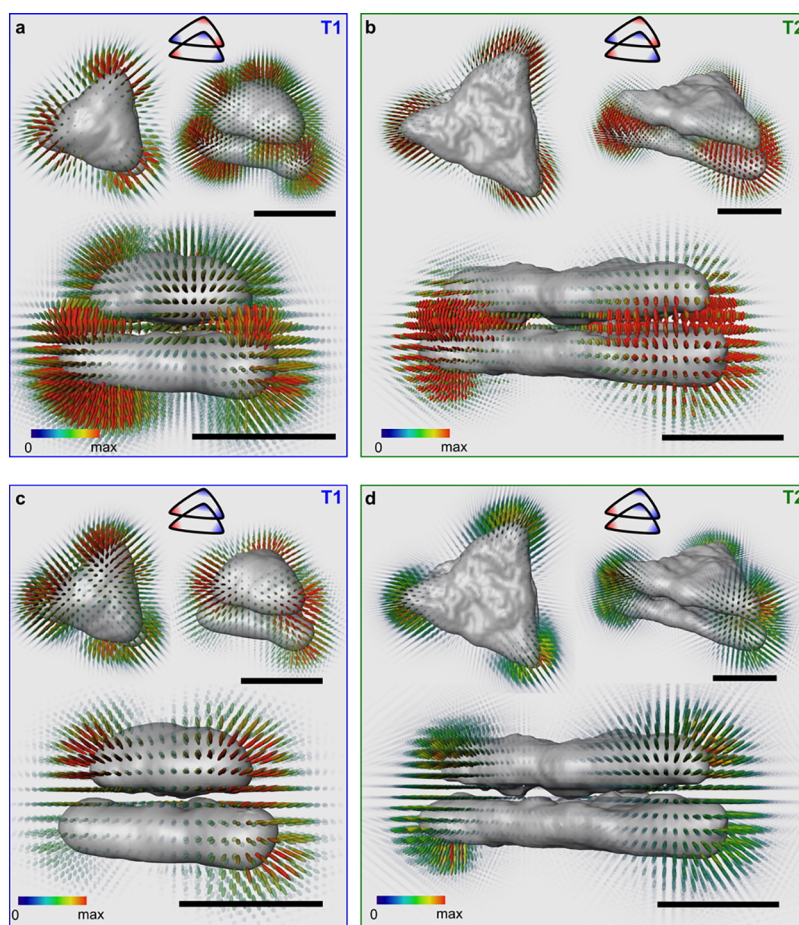


Figure 4. 3D reconstruction of the photonic LDOS: (a) Low-energy (bonding) mode of the dimer T1 and (b) T2. (c) High-energy (antibonding) mode of the dimer T1 and (d) T2. The orientation of the pencils indicates the direction along which the LDOS is maximal. Color, transparency, and length correspond to the magnitude of the full LDOS. The same color scale range is used for all modes to allow a relative comparison of their LDOS magnitude. The insets schematically show the charge distributions of the bonding and antibonding modes. Scale bars are 100 nm.

resonance energy of the individual lower triangle (see Figure S3). For the antibonding mode the LDOS is higher around the smaller upper triangle, as the energy of the antibonding mode is closer to the resonance energy of the individual upper triangle. A maximum of the LDOS in the gap region would be expected for triangles of exactly matching size.

In conclusion, we have experimentally observed vertical coupling by imaging the 3D LDOS distribution for two stacked nanotriangles. While the resulting bonding and antibonding configurations cannot be distinguished from 2D EELS maps, the unambiguous identification of coupled modes in stacked nanostructures only becomes possible thanks to plasmon tomography, which reveals the 3D photonic LDOS with nanometer resolution. This opens the path for the design and characterization of complex 3D plasmonic structures, tailored for applications in, for example, sensors. In addition, this approach is generally applicable to a wide range of plasmonic materials and may also be extended to investigate the coupling of plasmons to excitations in other materials, such as plasmon–exciton coupling with semiconductors. Finally, the high spatial resolution could be exploited to probe for quantum size effects in plasmonic structures.

■ ASSOCIATED CONTENT

📄 Supporting Information

The Supporting Information is available free of charge on the ACS Publications website at DOI: 10.1021/acs.nanolett.7b02979.

Movie showing the reconstructed photonic LDOS (AVI) Methods including sample preparation, EELS and HAADF STEM acquisition and processing, details about simulations and tomographic reconstruction of HAADF and EELS data (PDF)

■ AUTHOR INFORMATION

Corresponding Author

*E-mail: georg.haberfehlner@felmi-zfe.at.

ORCID

Georg Haberfehlner: 0000-0003-4136-9384

Notes

The authors declare no competing financial interest.

■ ACKNOWLEDGMENTS

This work has been supported by the European Union within the 7th Framework Program [FP7/2007-2013] under grant agreement no. 312483 (ESTEEM2), the Austrian Science Fund (FWF) projects P25034 and P27299-N27, and the FWF-SFB Nextlite, projects F4905-N23 and F4906-N23.

■ REFERENCES

- (1) Schuller, J. A.; Barnard, E. S.; Cai, W.; Jun, Y. C.; White, J. S.; Brongersma, M. L. *Nat. Mater.* **2010**, *9*, 193–204.
- (2) Chikkaraddy, R.; de Nijs, B.; Benz, F.; Barrow, S. J.; Scherman, O. A.; Rosta, E.; Demetriadou, A.; Fox, P.; Hess, O.; Baumberg, J. J. *Nature* **2016**, *535*, 127–130.
- (3) Wang, D.; Zhu, W.; Best, M. D.; Camden, J. P.; Crozier, K. B. *Nano Lett.* **2013**, *13*, 2194–2198.
- (4) Kollmann, H.; Piao, X.; Esmann, M.; Becker, S. F.; Hou, D.; Huynh, C.; Kautschor, L.-O.; Bösker, G.; Vieker, H.; Beyer, A.; Götzhäuser, A.; Park, N.; Vogelgesang, R.; Silies, M.; Lienau, C. *Nano Lett.* **2014**, *14*, 4778–4784.
- (5) Zhang, C.; Lu, Y.; Ni, Y.; Li, M.; Mao, L.; Liu, C.; Zhang, D.; Ming, H.; Wang, P. *Nano Lett.* **2015**, *15*, 1382–1387.
- (6) Zhu, W.; Esteban, R.; Borisov, A. G.; Baumberg, J. J.; Nordlander, P.; Lezec, H. J.; Aizpurua, J.; Crozier, K. B. *Nat. Commun.* **2016**, *7*, 11495.
- (7) Tan, S. F.; Wu, L.; Yang, J. K. W.; Bai, P.; Bosman, M.; Nijhuis, C. A. *Science* **2014**, *343*, 1496–1499.
- (8) Esteban, R.; Aguirregabiria, G.; Borisov, A. G.; Wang, Y. M.; Nordlander, P.; Bryant, G. W.; Aizpurua, J. *ACS Photonics* **2015**, *2*, 295–305.
- (9) Colliex, C.; Kociak, M.; Stéphan, O. *Ultramicroscopy* **2016**, *162*, A1–A24.
- (10) García de Abajo, F. J.; Kociak, M. *Phys. Rev. Lett.* **2008**, *100*, 106804.
- (11) Hohenester, U.; Ditlbacher, H.; Krenn, J. R. *Phys. Rev. Lett.* **2009**, *103*, 106801.
- (12) Hörl, A.; Trügler, A.; Hohenester, U. *Phys. Rev. Lett.* **2013**, *111*, 076801.
- (13) Nicoletti, O.; de la Peña, F.; Leary, R. K.; Holland, D. J.; Ducati, C.; Midgley, P. A. *Nature* **2013**, *502*, 80–84.
- (14) Hörl, A.; Trügler, A.; Hohenester, U. *ACS Photonics* **2015**, *2*, 1429–1435.
- (15) Hörl, A.; Haberfehlner, G.; Trügler, A.; Schmidt, F.-P.; Hohenester, U.; Kothleitner, G. *Nat. Commun.* **2017**, *8*, 37.
- (16) Su, K. H.; Wei, Q. H.; Zhang, X. *Appl. Phys. Lett.* **2006**, *88*, 063118.
- (17) Dmitriev, A.; Pakizeh, T.; Käll, M.; Sutherland, D. S. *Small* **2007**, *3*, 294–299.
- (18) Yankovich, A. B.; Verre, R.; Olsén, E.; Persson, A. E. O.; Trinh, V.; Dovner, G.; Käll, M.; Olsson, E. *ACS Nano* **2017**, *11*, 4265–4274.
- (19) Haberfehlner, G.; Orthacker, A.; Albu, M.; Li, J.; Kothleitner, G. *Nanoscale* **2014**, *6*, 14563–14569.
- (20) Haberfehlner, G.; Trügler, A.; Schmidt, F. P.; Hörl, A.; Hofer, F.; Hohenester, U.; Kothleitner, G. *Nano Lett.* **2015**, *15*, 7726–7730.
- (21) Duan, H.; Fernández-Domínguez, A. I.; Bosman, M.; Maier, S. A.; Yang, J. K. W. *Nano Lett.* **2012**, *12*, 1683–1689.
- (22) Nelayah, J.; Kociak, M.; Stéphan, O.; Geuquet, N.; Henrard, L.; García de Abajo, F. J.; Pastoriza-Santos, I.; Liz-Marzán, L. M.; Colliex, C. *Nano Lett.* **2010**, *10*, 902–907.
- (23) Schmidt, F. P.; Ditlbacher, H.; Hofer, F.; Krenn, J. R.; Hohenester, U. *Nano Lett.* **2014**, *14*, 4810–4815.
- (24) Hohenester, U.; Trügler, A. *Comput. Phys. Commun.* **2012**, *183*, 370–381.
- (25) Hohenester, U. *Comput. Phys. Commun.* **2014**, *185*, 1177–1187.
- (26) Sauvan, C.; Hugonin, J. P.; Maksymov, I. S.; Lalanne, P. *Phys. Rev. Lett.* **2013**, *110*, 237401.
- (27) García de Abajo, F. J. *Rev. Mod. Phys.* **2010**, *82*, 209–275.